

## Wave tank study of particulate organic matter degradation in permeable sediments

Ulrich Franke,<sup>1</sup> Lubos Polerecky, Elimar Precht,<sup>2</sup> and Markus Huettel<sup>3</sup>

Max Planck Institute for Marine Microbiology, Celsiusstrasse 1, D-28359 Bremen, Germany

### Abstract

We used a wave tank to study the influence of pore-water flow and diffusive transport on the degradation of labile particular organic matter (POM: *Ulva lactuca* pieces) embedded in permeable sediment. Pore-water advection, induced by the interaction of the wave-driven oscillatory boundary flow and stationary sediment ripples, reproducibly exposed POM buried in the top 2 cm of the sediment to oxic or anoxic conditions lasting between days and weeks. Planar oxygen optodes together with carbon and nitrogen analyses were used to visualize and quantify the degradation rates. Oxygen consumption rates (OCR) were up to 18-times higher at locations of the buried POM compared to the surrounding sediment. Elevated OCR were also detected downstream the POM locations. Despite high permeability of the sediment and exposure to oxygenated pore-water flows, suboxic and anoxic sites and suboxic pore-water “plumes” developed at and downstream of the locations of POM in otherwise oxygenated sediment regions. The carbon loss of the buried *U. lactuca* discs derived from the OCR measurements was only 4–15% of that measured by the carbon analysis of the recovered pieces, suggesting that the bacterial degradation of POM and the final degradation of dissolved organic matter (DOM) were spatially decoupled by the pore-water flow. Advection can thus enhance the rate of organic matter degradation by efficiently distributing DOM from the “hotspots” of organic matter mineralization to larger volumes of permeable sediments and associated microbial communities.

Permeable sediments are abundant in the global continental shelf regions (Emery 1968). These nonaccumulating sands are generally poor in organic carbon and have been considered long time as relatively inactive habitats that do not contribute substantially to the cycling of organic matter (Boudreau et al. 2001). Recent studies, however, indicate that the low concentration of organics is more likely the result of rapid turnover and high exchange rates (Huettel et al. 1998; Rusch et al. 2003). When the interaction of the boundary-layer flow (e.g., unidirectional or oscillatory flow induced by currents and gravity surface waves, respectively) and sediment topography enables dynamic advective pore-water flow, the solute exchange at the sediment-water interface can exceed transport by molecular diffusion by several

orders of magnitude (Rutgers van der Loeff 1981; Precht and Huettel 2004; Reimers et al. 2004). Advection can significantly increase the oxygen penetration depths in sediments (Forster et al. 1996; Lohse et al. 1996; Ziebis et al. 1996a) as well as the transport of organic particles (Huettel et al. 1996; Rusch and Huettel 2000), resulting in enhanced sedimentary oxygen consumption and organic matter degradation (Forster et al. 1996; Ziebis et al. 1996b; Reimers et al. 2004).

The increased degradation activity in advective sedimentary systems is most likely the result of several factors. Transport of nutrients towards the sedimentary bacteria, which can be the limiting factor under stagnant, diffusive-dominated conditions, is enhanced by fluid motion (van Loosdrecht et al. 1990). Furthermore, efficient directed transport of oxygen and other electron acceptors as well as organic matter from the overlying water to the sedimentary community, combined with fast transport of inhibitory products like ammonia and sulphide out of the sediment, can enhance bacterial activity under advection (Ziebis et al. 1996b; Huettel et al. 1998).

The biogeochemical reactions in the sediment and advective transport of organic particles and solutes result in a complex three-dimensional zonation of oxygen, organic material, nutrients, and heavy metals. In contrast to many diffusion-dominated sediments, this zonation is highly dynamic, as it is tightly linked to rapidly changing sediment topography and overlying water flow (Ziebis et al. 1996b; Huettel et al. 1998; Precht et al. 2004). Metabolic activity at the transition between oxic and anoxic zones is considered to be very intensive, especially when these zones show temporal or spatial oscillations (Aller 1994; Huettel et al. 1998).

Total sediment mineralization can be estimated from the measurements of benthic oxygen uptake (Thamdrup and Canfield 2000). This approach is applicable in systems, e.g., cohesive sediments, where minor electron sinks, such as the

<sup>1</sup> Present address: FAB Anlagenbau GmbH, Ostarstr. 5, 51107 Cologne, Germany (u.franke@fab-anlagenbau.com).

<sup>2</sup> Present address: DHI Wasser & Umwelt, Wiesenstrasse 10A, D-28857 Syke, Germany

<sup>3</sup> Present address: Florida State University, Department of Oceanography, 0517 OSB, West Call Street, Tallahassee, Florida 32306-4320.

### Acknowledgments

We thank Björn Grunwald and Gerhard Holst for assistance with the MOLLI system. Ingo Klimant (Institute for Analytical Chemistry, Micro- and Radiochemistry, Technical University of Graz, Austria) and Claudia Schröder (Institute for Analytical Chemistry, Bio- and Chemo-Sensors, University of Regensburg, Germany) are thanked for the recipe, the technical advice, and help with the preparation of planar O<sub>2</sub> optodes. Bo Barker Jørgensen is acknowledged for constant interest and support of this work, Dirk de Beer for valuable comments and discussion. Georg Herz, Alfred Kutsche, Volker Meyer, and Paul Färber are acknowledged for their help with the wave tank setup and electronics. Valuable comments of Ronnie Glud and two anonymous reviewers are much appreciated. The study was funded by the German Federal Ministry of Education and Research (BMBF, project 03F0284A) and the Max Planck Society (MPG).

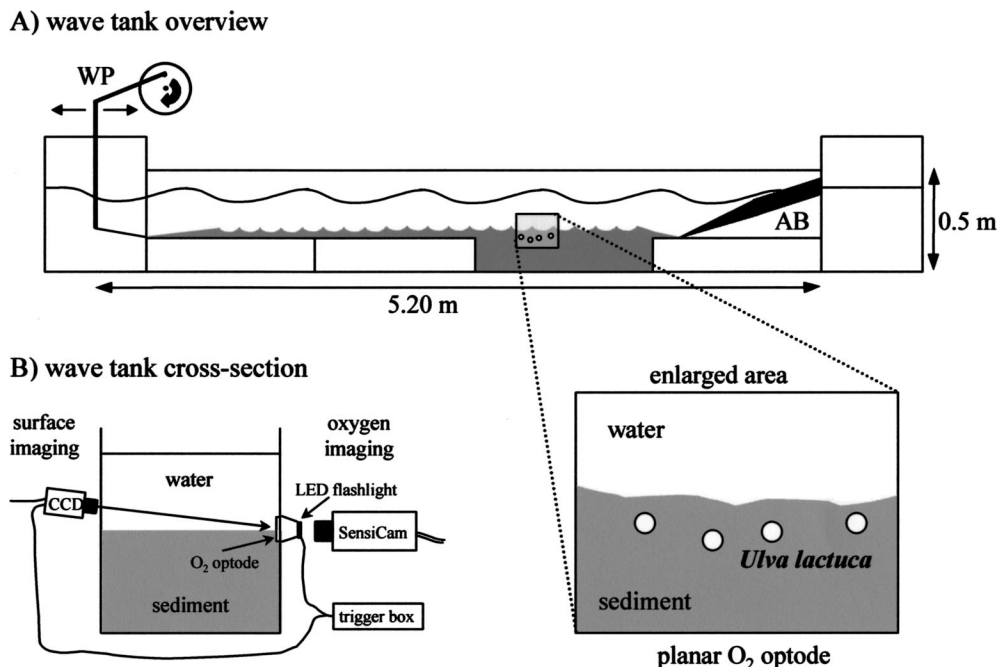


Fig. 1. The experimental wave tank setup. (A) Overview with locations of circular pieces of *U. lactuca* placed in the sediment in front of the semi-transparent planar  $O_2$  optode, preferably under ripple troughs; WP = wave paddle, AB = artificial beach. (B) Cross-section of the wave tank showing the setup for the simultaneous sediment surface and oxygen imaging.

release of dinitrogen and permanent burial of metal sulfides, can be ignored, as oxygen is the terminal electron acceptor for benthic degradation processes of organic matter (Canfield et al. 1993). In permeable sediments, oxygen consumption is typically determined by sealable sediment enclosures in which close to natural flow conditions can be mimicked. Typical examples include flume setups (Forster et al. 1996; Ziebis et al. 1996b) or diverse benthic chambers used under laboratory or in situ conditions (e.g., Malan and McLachlan 1991; Huettel and Gust 1992; Glud et al. 1996a). Other, more recent approaches include flow-through sediment column systems (Reimers et al. 2004; de Beer et al. 2005; Polerecky et al. 2005) and the in situ eddy-correlation technique (Berg et al. 2003). The method of Polerecky et al. (2005) can give insight into the small scale spatial distribution of two-dimensional oxygen consumption rates (OCR) in the sediment, which is impossible to assess with the other methods. This was enabled by the use of a planar oxygen optode, introduced to marine systems by Glud et al. (1996b), which allows two-dimensional oxygen measurements in the sediment with a high spatio-temporal resolution. Planar oxygen optodes have been used successfully to measure oxygen dynamics and distributions in diverse marine applications (e.g., Glud et al. 1999; Precht et al. 2004; Wenzhöfer and Glud 2004).

This study aims to assess the spatial and temporal variability of aerobic degradation of particular organic matter (POM) buried in permeable sediment, and to investigate the influence of different transport modes (advective vs. diffusive) on the degradation rates. Experiments were conducted in a wave tank so as to mimic natural conditions. Planar oxygen optodes allowed the estimation of the aerobic POM

degradation without disturbing the samples, the sediment, or the degradation conditions. The planar optode measurements were supplemented with carbon and nitrogen analyses, providing a direct quantification of the degradation of the POM samples removed from the sediments. By comparing these two approaches, a possible mechanism by which advection can enhance the POM degradation could be identified.

## Materials and methods

**Wave tank setup**—Experiments were carried out in a laboratory wave tank setup identical to that described by Precht et al. (2004) (Fig. 1A). The wave tank was filled with natural sandy sediment (median grain size  $180 \mu\text{m}$ , porosity 35.2%, permeability  $13.0 \pm 0.3 \times 10^{-12} \text{ m}^2$ ) and artificial seawater (salinity 32). Over a period of  $\sim 1$  year prior to our experiments, extensive advective process studies were conducted (Precht et al. 2004), during which food (powdered dried red algae, equivalent to an input of  $1 \text{ g m}^{-2}$ ) was added biweekly to the sediment. The nourishment was stopped three weeks before our experiments. Organic carbon (C) and nitrogen (N) contents of the top 5 cm of sediment, analysed using a Fisons NCS 1500 elemental analyzer, were  $800 \pm 25$  ( $n = 5$ ) and  $30 \pm 9$  ( $n = 5$ )  $\mu\text{g g}^{-1}$  dry weight, respectively. Neither oligochaetes nor active microphytobenthos were present in the sediment, as concluded from the missing burrowing activity at the sediment surface and no oxygen increase after long illumination periods, respectively. The top sediment horizon (1–3 cm thick) was frequently oxygenated by advection, while the deeper sediment layers remained reduced.

Sediment surface topography was created by sinusoidal

waves generated at the upstream end of the wave tank using a wave paddle (Fig. 1A, see Precht et al. (2004) for further details). In particular, propagating ripples were produced by adjusting the water level to a height ( $h$ ) of 19 cm above the sediment surface and the wave amplitude ( $a$ ) to 7 cm, wavelength ( $\lambda$ ) to 70 cm and frequency ( $f$ ) to 1.25 Hz (settings 1). With these settings, root mean square value of the horizontal flow velocity directly above the sediment was  $U_{\text{RMS}} \sim 0.12 \text{ m s}^{-1}$ , as measured with a three-beam DANTEC<sup>™</sup> LDA (Laser Doppler Anemometer). When the settings were changed to  $h = 15 \text{ cm}$ ,  $a = 5 \text{ cm}$ ,  $\lambda = 80 \text{ cm}$  and  $f = 1.1 \text{ Hz}$  (settings 2), resulting in  $U_{\text{RMS}} \sim 0.08 \text{ m s}^{-1}$ , the formed ripples remained stationary.

**Two-dimensional oxygen distributions**—Two-dimensional (2D) oxygen distributions were measured with a semi-transparent planar oxygen optode (14 cm wide, 10 cm high) glued to the wave tank wall by transparent silicone (Elastosil<sup>®</sup> E4, Wacker). The optode was prepared as described in Precht et al. (2004). The sensing layer (30  $\mu\text{m}$  thick) was made from a solution containing 10 mg of fluorophore Platinum(II) meso—tetra (pentafluoro-phenyl) porphyrin (Pt-PFP) (Porphyrin Products), 490 mg Polystyrene (Sigma-Aldrich), 3 mL Chloroform (Merck) and 330 mg titanium dioxide ( $\text{TiO}_2$ ) particles (<5  $\mu\text{m}$ , Aldrich). Oxygen images were recorded using the luminescence lifetime imaging system (Holst et al. 1998; Holst and Grunwald 2001), which is based on the dynamic quenching of fluorophore's luminescence lifetime by oxygen (Kautsky 1939). The accuracy of oxygen readings was between 2% air saturation (AS) and 7% AS in the regions of 0–10% AS and 75–100% AS, respectively. The images (640  $\times$  480 pixels) covered an area of 80  $\times$  60 mm, resulting in a spatial resolution of 125  $\times$  125  $\mu\text{m}$  pixel<sup>-1</sup>. The oxygen images were superimposed with the sediment surface images recorded synchronously using a second CCD camera mounted on the other side of the wave tank channel (Fig. 1B) (Precht et al. 2004).

**2D oxygen consumption rate (OCR) measurements**—Oxygen was transported into the sediment by advection induced by the interaction of the overlaying water flow and the sediment topography (Precht et al. 2004). Initial steady state oxygen distributions, denoted as  $c_i$ , were achieved by producing waves for a period of 3–5 h (using settings 2, see previous). After the waves were stopped, oxygen transport in the sediment was governed by molecular diffusion and the initial oxygen dynamics was formally described by the diffusion equation  $(\partial c/\partial t)_i = D_s \Delta c_i - R$ . Here,  $D_s \Delta c_i$  represents the diffusive transport in the sediment characterised by the diffusion coefficient  $D_s$  and  $R > 0$  is the local OCR (note that  $R < 0$  would describe oxygen production rate) (Crank 1975). Rearranging this equation,  $R$  can be calculated as

$$R = D_s \Delta c_i - (\partial c/\partial t)_i \quad (1)$$

Since both  $D_s \Delta c_i$  and  $(\partial c/\partial t)_i$  are calculated from oxygen images measured by the planar optode at the wall,  $R$  in Eq. 1 represents the local OCR at or close to the wall.

The time series of oxygen images recorded every 30 s for 50 min after the waves were stopped were used to quantify

$(\partial c/\partial t)_i$ . The concentrations in each pixel were fitted by the most suitable polynomial (order between 0 and 4), and the initial time-derivative of the fit was taken as the value of  $(\partial c/\partial t)_i$  in the corresponding pixel (see Polerecky et al. 2005 for details of the fitting procedure). The diffusive term  $D_s \Delta c_i$  in Eq. 1 was determined from the 2D oxygen distribution measured immediately ( $\sim 2$ – $5 \text{ s}$ ) before the waves were stopped. Since the effect of the wall (planar optode) on the diffusion in porous medium could not be accurately determined, two effective diffusion coefficients were used, namely  $D_{s1} = (\phi/\theta^2) \times D_w = 0.21 \times 10^{-9} \text{ m}^2 \text{ s}^{-1}$  and  $D_{s2} = D_w = 1.83 \times 10^{-9} \text{ m}^2 \text{ s}^{-1}$ .  $D_{s1}$  was calculated according to Boudreau (1996), taking into account the sediment porosity ( $\phi = 35.2\%$ ) and tortuosity ( $\theta^2 = 1 - \ln(\phi^2) = 3.1$ ).  $D_w$  is the diffusion of oxygen in seawater corrected for salinity (32) and temperature (17°C) (Li and Gregory 1974). The term  $\Delta c_i = \partial^2 c_i/\partial x^2 + \partial^2 c_i/\partial y^2$  was calculated using the 2D Savitzky-Golay smoothing algorithm (Krumm 2001: <http://research.microsoft.com/users/jckrumm/SavGol/SavGol.htm>). All calculations were implemented in Matlab<sup>®</sup>.

**Particular organic matter**—Samples of *U. lactuca* were provided from the Alfred Wegener Institute for Polar and Marine Research (Helgoland Island), stored in artificial seawater (instant sea<sup>™</sup>, salinity 32, temperature 15°C) under 12 h light/12 h dark conditions. Circular pieces (diameter  $\varnothing$  5 mm, dry weight 900–1,200 mg) of *U. lactuca* were cut from a fresh large thallus and served as POM in the experiments.

## Experimental procedure

Sediment ripples were generated using the wave tank settings 1 (see previous). Subsequently, 4 circular pieces of *U. lactuca* were placed directly flat against the optode at a sediment depth of 0.5–1.5 cm. The *Ulva* pieces were placed under the ripple troughs (Fig. 1A), and the wave tank settings 2 were adjusted (sediment ripples remained stationary, see previous), which enabled easy manipulation of the oxygen content under the ripple troughs and the locations of the *Ulva* by turning on and off the wave action that controlled the advective pore-water exchange (Precht et al. 2004).

Three degradation scenarios, each characterized by different redox conditions prevailing during the degradation, were investigated (Fig. 2). In Experiment 1, the *U. lactuca* discs and the sediment surrounding them were kept continuously oxic and under advection-dominated conditions. The exceptions were the five OCR measurements conducted at 6-d intervals, when the waves were stopped for approx. 1 h. In Experiment 2, *U. lactuca* and the surrounding sediment were maintained under anoxic and diffusion-dominated conditions (no waves). The exceptions were the three OCR measurements performed on days 0, 12, and 24, when the waves were switched on for 3–5 h in order to oxygenate the sediment allowing the measurement of its depletion rate by the planar optode technique (see previous). In Experiment 3, *U. lactuca* and the surrounding sediment were kept under alternating oxic (advection-dominated) and anoxic (diffusion-dominated) conditions of three days each. OCR measurements were performed every 3 days.

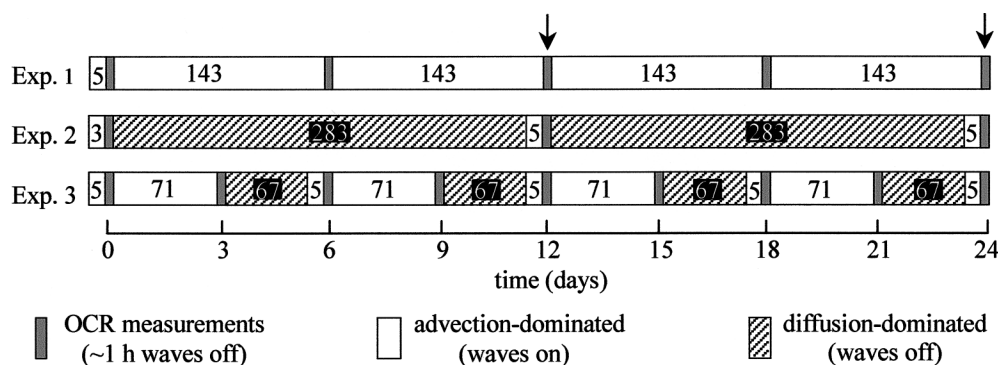


Fig. 2. Time-protocols of the three degradation experiments specifying the conditions of *Ulva lactuca* and the surrounding sediment. Arrows indicate the time (after the OCR measurements) at which 1–2 discs of *U. lactuca* were removed for the carbon and nitrogen analyses. The duration (h) of the advective- and diffusive- conditions is indicated by the numbers insight the panels. OCR measurements in each experiment lasted ~1 h.

### Analytical procedures

**Plant material**—Wave tank degradation experiments: A direct measurement of the total carbon and nitrogen loss of the buried *U. lactuca* pieces was done using a Fisons NCS 1500 elemental analyzer. After 12 d and at the end of each experiment (Fig. 2), 1–2 *U. lactuca* pieces were removed from the sediment and dried overnight at 60°C. Each disc was cut into 4 pieces and analyzed for total carbon and nitrogen content. The control experiments were done by applying the same procedure to freshly cut *U. lactuca* stored in aerated, artificial seawater in the dark at 17°C for the same periods.

**Test tubes DOC experiment:** An additional control experiment was conducted to test whether DOC was produced by *U. lactuca* itself, by bacteria already attached to it, or by bacteria living in the sediment. *U. lactuca* discs ( $\varnothing$  5 mm) were placed at the wall of 21 test tubes (10 mL) and covered with ~1 cm<sup>3</sup> sterile sediment and 5 mL of artificial nonsterile seawater (salinity 32). Test tubes without algae served as controls. Every third day, *U. lactuca* discs were removed from 3 test tubes. The sediment was mixed by a vortex shaker and allowed to settle for 5 min. The water from each test tube was decanted into a 10 mL syringe, filtered through a nylon filter (Millex-GN Filter Unit, Millipore, pore size 0.2  $\mu$ m) and kept frozen at –20°C until analysis. The DOC analysis was conducted using a Shimadzu TOC-5050A total organic carbon analyzer, which determines the total dissolved carbon (TDC) and dissolved inorganic carbon (DIC). DOC was calculated by subtracting DIC from TDC.

**Calculations of consumed carbon from OCR**—The amount of carbon mineralized during the wave tank experiments deduced from the time-series of OCR measurements (Fig. 2) was calculated by the following procedure. First, the measured OCR was converted into carbon mineralization rate (CMR) according to Florek and Rowe (1983) as

$$\text{CMR (ng cm}^{-3} \text{ day}^{-1}) = \text{OCR (ng cm}^{-3} \text{ day}^{-1}) \times 12/32 \times \text{RQ} \quad (2)$$

assuming a simplified reaction  $\text{CH}_2\text{O} + \text{O}_2 \rightarrow \text{CO}_2 + \text{H}_2\text{O}$

for the organic matter degradation and a respiratory quotient (RQ) of 0.85 (Rowe et al. 1994). The factor 12/32 takes into account the carbon: oxygen molar weight ratio.

Second, it was assumed that the OCR measured at locations of the *Ulva* discs were not limited only to the immediate vicinity of the algae but extended over a half sphere of the disc diameter into the sediment ( $\varnothing = 0.5$  cm; volume  $\Delta V = 0.033$  cm<sup>3</sup>). The CMR per disc of *U. lactuca* (ng disc<sup>-1</sup> day<sup>-1</sup>) could then be calculated by multiplying the volumetric CMR in Eq. 2 with the volume  $\Delta V$ . The same procedure was applied to the OCR of the sediment in central areas under ripple troughs to allow a direct comparison with the CMR at the *Ulva* locations. Finally, the time-series of the CMR values were integrated over 24 d to estimate the total amount of carbon mineralized over the entire experimental period.

### Results

**Steady state oxygen distributions**—Steady state oxygen distributions maintained under long-term advective conditions were similar in all experiments (Fig. 3A, C, D). Characteristic undulating patterns of oxygen-rich pore water developed under ripple troughs and oxygen depleted pore-water upwelling zones formed under ripple crests (Precht et al. 2004). Oxygen penetration was enhanced under ripple troughs (0.5–2.4 cm), and strong vertical as well as horizontal oxygen gradients developed (Table 1, Fig. 3). When diffusive conditions lasted for more than 4 h, oxygen was completely consumed in deeper sediment layers and its penetration was limited to the top 0.5–0.7 cm (Fig. 3, Table 1). Under these conditions, oxygen distributions in experiments 3 (Fig 3B) and 2 (data not shown) were very similar.

Figures 3C and 3D demonstrate that steady local zones of reduced oxygen concentrations (5–70  $\mu$ mol L<sup>-1</sup>) developed at the locations of the *U. lactuca* discs as well as in the sediment downstream the discs. This was caused by the enhanced oxygen consumption at the *Ulva* discs, which compared in magnitude to the advective oxygen supply. In contrast, no such oxygen-reduced zones were observed in the

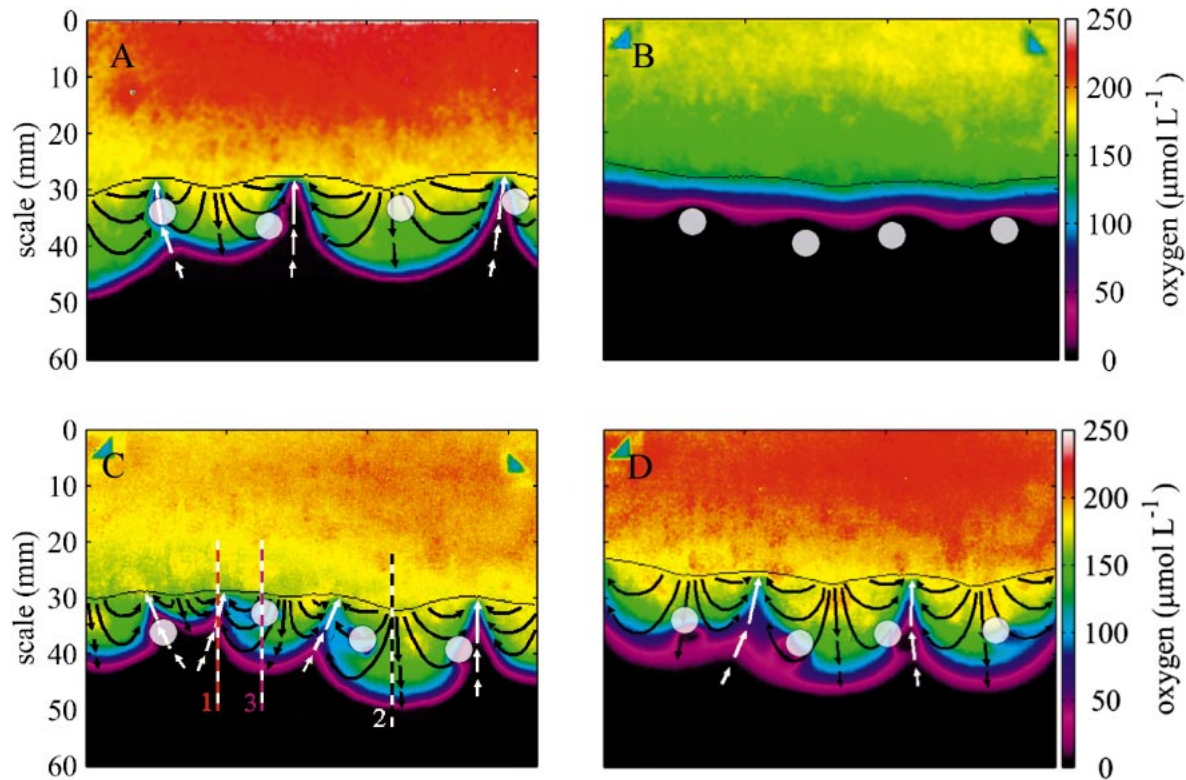


Fig. 3. Quasi-steady-state oxygen distributions maintained during the long-term degradation experiments under advection (oxic) and diffusion (anoxic) conditions, respectively. Panels A, C, and D show typical steady state oxygen distributions under advective conditions prior to OCR measurements conducted during Exp. 1, 2, and 3, respectively. Panel B shows exemplarily a typical steady state oxygen distribution during long term diffusive conditions in Exp. 3. Circles show the positions of *U. lactuca* discs, black horizontal lines the sediment surface, and the arrows indicate the approximate streamlines of the porewater flow estimated according to Shum and Sundby (1996). Vertical lines 1–3 in panel C indicate three selected sediment regions from which vertical oxygen profiles were extracted and plotted as a function of time in Fig. 4.

surrounding sediment, where the oxygen consumption was relatively low.

**Oxygen dynamics**—To illustrate the qualitatively different dynamic behavior of oxygen distributions and penetration depths in the sediment under alternating advective and diffusive conditions, selected vertical oxygen profiles were extracted from the oxygen images and plotted as a function of time (Fig. 4; see also Fig. 3C for the positions of the extracted profiles). Below ripple crests, anoxic pore water was initially driven towards the sediment surface after the wave-

induced transition from diffusion- to advection-dominated conditions (Fig. 4A, left panel). With time, the upwelling water became gradually mixed with oxygen-rich pore water coming from the ripple flank, resulting in a slow increase of the oxygen penetration depth. Due to the absence of advection-driven upwelling of anoxic pore water after the waves were stopped (Fig. 3A, right panel), oxygen was transported deeper into the sediment by diffusion. Below ripple troughs, oxygen was pushed rapidly deeper into the sediment after the onset of advective transport (Fig. 4B, left panel), whereas oxygen penetration slowly decreased after the advection was stopped and the transport was dominated by diffusion (Fig. 4B, right panel).

The situation was qualitatively different when *U. lactuca* was present under a ripple trough. After the transition from the diffusion- to advection-dominated conditions (Fig. 4C, left panel), the initial rapid advection-driven increase of oxygen penetration into the sediment was temporally stopped after ~20 min at the position of the *Ulva* disc. This was caused by the elevated oxygen consumption that exceeded the mainly downward advective supply. Due to the three-dimensional transport characteristics of the pore-water flow, oxygen was gradually transported below the *U. lactuca* disc from the surrounding sediment. However, a local suboxic

Table 1. Summary of the ripple wavelengths, ripple amplitudes, and typical maximum oxygen penetration depths during the experiments.

Exp.	Ripple wavelengths (cm)	Ripple amplitudes (cm)	Typical oxygen penetration depths under	
			Advection (cm)	Diffusion (cm)
1	2.5–4.0	0.1–0.4	1.3–2.4	0.5–0.7
2	1.4–2.5	0.1–0.3	0.5–1.8	0.5–0.7
3	~2.7	0.2–0.4	1.8–2.0	0.5–0.7

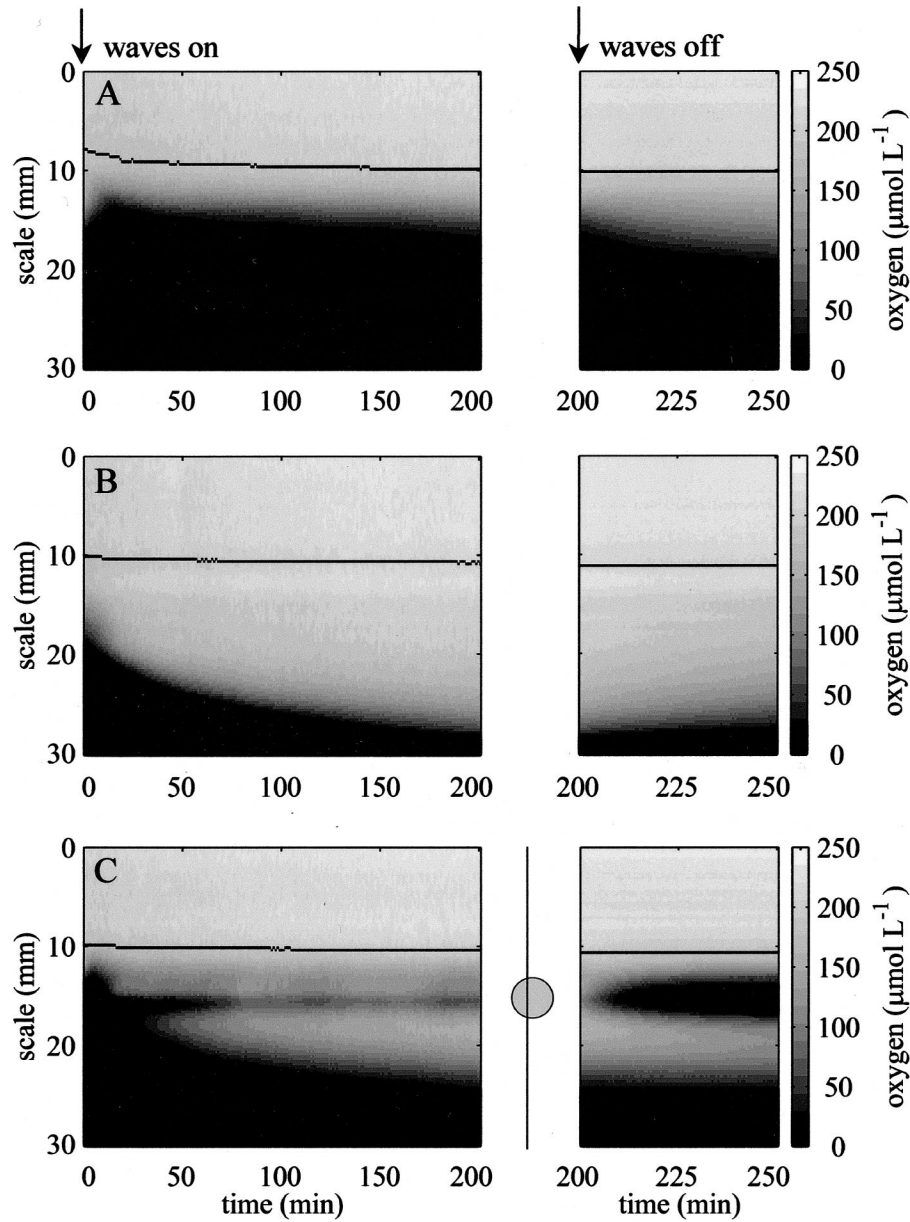


Fig. 4. Typical time evolutions of selected vertical oxygen profiles in the sediment with freshly buried POM after an abrupt change of the transport conditions from diffusion- to advection-dominated (left panels) and from advection- to diffusion-dominated (right panels). The respective abrupt changes were induced by switching the waves on and off at times indicated by arrows. The positions of the profiles in panels A, B, and C are indicated in Fig. 3C by the vertical lines 1, 3, and 2, respectively. The circle and the vertical line in panel C indicate the location of the *U. lactuca* disc in the sediment and the relative position of the extracted profile with respect to *Ulva*, respectively. The black horizontal lines show the sediment surface. The greyscale was adjusted so as to enhance the contrast at lower oxygen concentrations. Note that the widths of the figures are not to scale.

region ( $<70 \mu\text{mol L}^{-1}$ ) remained at the position of the *U. lactuca* disc during the entire advective period. After the waves were stopped (Fig. 4C, right panel), the removal of oxygen was considerably faster at the location of the *U. lactuca* disc, where anoxia was reached within 15–70 min, depending on the experiment. The presence of *Ulva*, thus, resulted in reversed oxygen gradients in deeper sediment during both advective and diffusive conditions.

The oxygen dynamics under advective and diffusive con-

ditions are more clearly demonstrated in movies produced from temporal sequences of the oxygen images that can be found in Web Appendix 1 ([http://www.aslo.org/lo/toc/vol\\_51/issue\\_2/1084a1.html](http://www.aslo.org/lo/toc/vol_51/issue_2/1084a1.html)). The movies show the development of steady state oxygen distribution beneath stationary sediment ripples after the *U. lactuca* discs were placed in the sediment and the waves were switched on, as well as the oxygen dynamics after the waves were stopped (corresponding to Fig. 3).

Table 2. OCR values ( $\mu\text{mol L}^{-1} \text{min}^{-1}$ ) averaged over selected *U. lactuca* discs ( $\sim 5$  mm diameter), calculated without (column 2) and with (columns 3 and 4) diffusion correction. The standard deviations indicate the variability of the OCR values within the averaged area.

Exp.	$R = -(\partial c/\partial t)_i$	Eq. 1 using $D_{s1}$	Eq. 1 using $D_{s2}$
1	$4.5 \pm 1.8$	$4.9 \pm 2.3$	$5.1 \pm 2.4$
2	$5.8 \pm 3.0$	$5.9 \pm 3.6$	$6.1 \pm 4.0$
3	$2.9 \pm 1.2$	$3.0 \pm 1.7$	$3.2 \pm 2.5$

**2D OCR measurements**—The correction of the OCR images for diffusion (Eq. 1) did not produce satisfactory results using neither with  $D_{s1}$  nor with  $D_{s2}$  (data not shown). When the lower ( $D_{s1}$ ) value was used, the R image still contained areas with apparent oxygen production under the ripple crests. On the other hand, the higher value ( $D_{s2}$ ) resulted in occasional patches of apparent oxygen production in areas under the ripple troughs, which was also unacceptable. The possible reasons for these artefacts could be twofold. Heavy smoothing had to be applied to the rather noisy oxygen images (2D Savitzky-Golay Filter, polynomial of order 3, patch size of  $17 \times 17$  pixels), which could have lowered  $\Delta c_i$  in pixels where oxygen gradients varied abruptly (e.g., under the ripple crests). On the other hand, the value of  $D_{s2}$  was probably too high to describe diffusion in a porous medium near a wall.

Nevertheless, the systematic error introduced to the OCR values at the locations of *U. lactuca* discs by not including the diffusion-correction, i.e., by calculating the OCR image from  $R = -(\partial c/\partial t)_i$  (compare to Eq. 1), did not exceed 10–15% (Table 2). Since the initial 2D oxygen distributions of the OCR measurements were very similar for each experiment (data not shown), this inaccuracy was the same for each calculated OCR image. Because the minor underestimation of the OCR values does not influence the main conclusions of our study, only the diffusion-uncorrected OCR values ( $R = -(\partial c/\partial t)_i$ ) will be presented below.

Typical OCR images are shown in Fig. 5. The positions of *U. lactuca* discs were clearly visible as areas of significantly elevated OCR values compared to the surrounding sediment. These areas were slightly larger ( $\varnothing 7.1$ – $8.8$  mm) than the actual size of the *U. lactuca* discs ( $\varnothing 5$  mm). When the *Ulva* discs were removed (day 12 of the experiments), the regions of increased OCR disappeared (Fig. 5D). Peak sediment OCR values appeared at the transition zones between the oxic and anoxic sediment areas as well as close to *U. lactuca* discs. Lowest sediment OCRs were measured in the central areas of ripple troughs.

The OCR values were averaged over circular areas ( $\varnothing 5$  mm) either at the locations of *U. lactuca* or in the central area under the ripple troughs for all conducted OCR measurements summarised in Fig. 2, and are shown in Fig. 6A. At the locations of *U. lactuca* discs, OCR decreased expo-

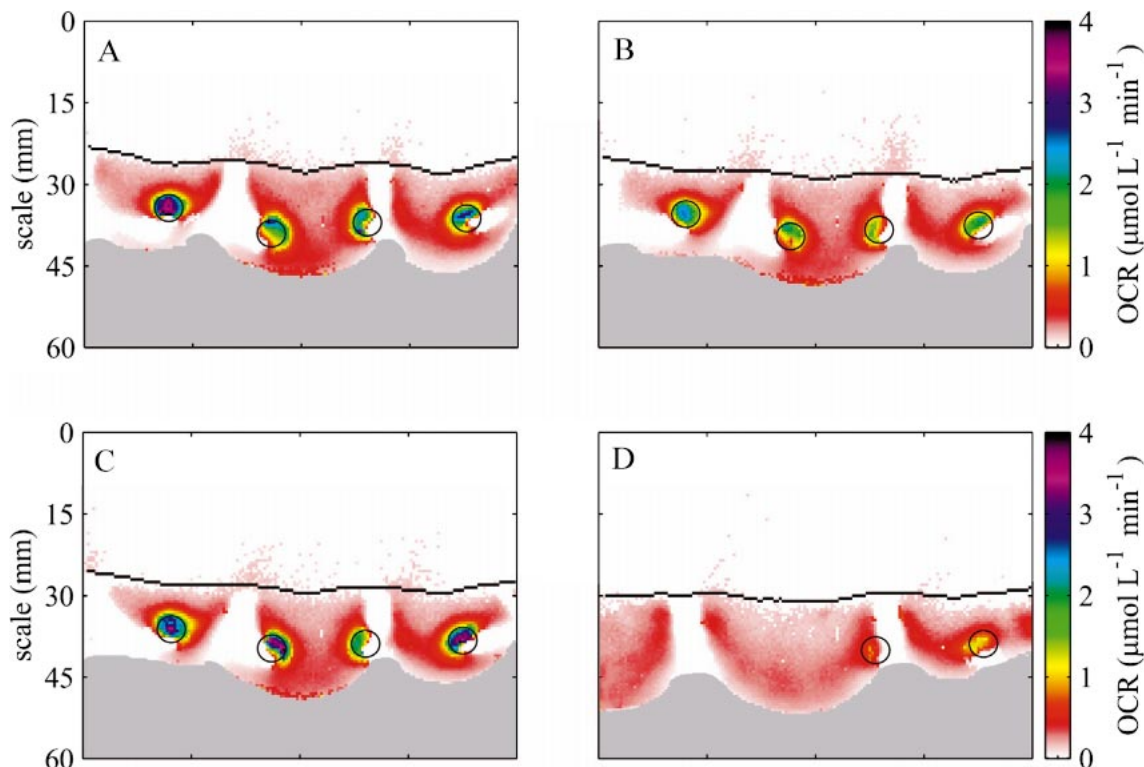


Fig. 5. Typical examples of the calculated OCR images. Images A, B, C, and D correspond to the OCR measurement number 1 (day 0), 2 (day 3), 3 (day 6), and 6 (day 15) of Experiment 3, respectively (see Fig. 2). OCR values are expressed per volume of porewater. Black horizontal lines indicate the sediment surface, and circles show the locations of *U. lactuca* discs. Grey regions indicate deep sediment areas where no  $(\partial c/\partial t)_i$  was measurable due to the lack of oxygen, whereas white regions in the sediment correspond to areas with  $(\partial c/\partial t)_i > 0$ .

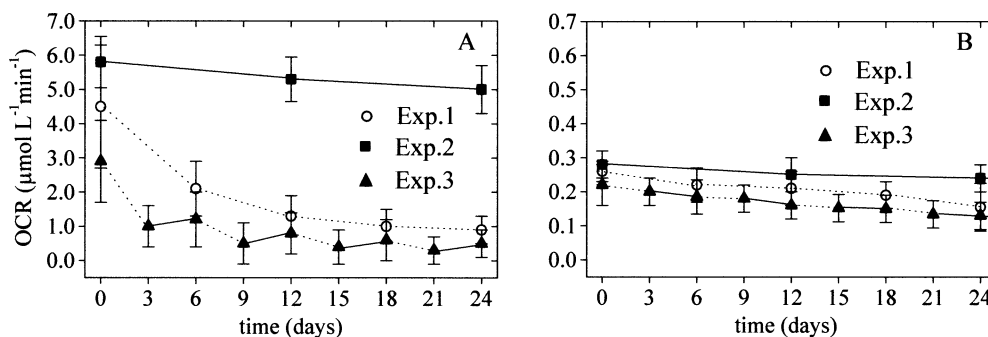


Fig. 6. OCR values averaged over circular areas (5 mm diameter) at locations of (A) *U. lactuca* and (B) in the central area under the ripple troughs. Error bars indicate the variability of the OCR over the averaged area. Solid and dotted lines represent the long-term anoxic and oxic periods preceding the OCR measurements, respectively. Note different scaling of panels A and B.

nentially (from  $\sim 4.5$  to  $\sim 1.0 \mu\text{mol L}^{-1} \text{min}^{-1}$ ) under long-term oxic conditions (Exp. 1), whereas the values changed only slightly (from  $\sim 5.6$  to  $\sim 5.0 \mu\text{mol L}^{-1} \text{min}^{-1}$ ) when the degradation took place during prolonged anoxic conditions (Exp. 2). In Experiment 3, OCR decreased rapidly and increased slightly after the *Ulva* pieces were exposed to oxic and anoxic conditions, respectively. The overall decrease of OCR in this experiment was approx. exponential (from  $\sim 3.0$  to  $\sim 0.5 \mu\text{mol L}^{-1} \text{min}^{-1}$ ; Fig. 6A).

In contrast, only minor decreases (from  $0.22$ – $0.29$  to  $0.15$ – $0.25 \mu\text{mol L}^{-1} \text{min}^{-1}$ ) in the sedimentary OCR were observed during the 24-d duration of the three experiments (Fig. 6B). The OCR were approx. 10–20 times lower than those at positions of *Ulva* pieces measured at the beginning of each experiment or during the entire Experiment 2. At the end of experiments with prolonged oxic conditions (Exp. 1 and 3), the sediment values were only around 2–3 times smaller than the OCR at the locations of *U. lactuca*.

*Ulva lactuca* analyses—Neither discs of *U. lactuca* taken out of the wave tank sediment for analysis after 12 and 24 d, nor the *U. lactuca* pieces from the test tubes experiment, nor the controls stored in nonsterile artificial seawater changed significantly their appearance during the experiments, and all looked intact and greenish.

Wave tank degradation experiment: Carbon (C) and nitrogen (N) contents of *U. lactuca* varied considerably in all experiments. Carbon values ranged from  $204$  to  $531 \text{ mg C g}^{-1}$  dry weight (dw) with standard deviations (SD) of  $30$ – $112 \text{ mg C g}^{-1} \text{ dw}$  ( $n = 4$ ). Nitrogen content of single discs varied between  $9$  and  $26 \mu\text{g N g}^{-1} \text{ dw}$  ( $\text{SD} = 1$ – $4 \mu\text{g N g}^{-1} \text{ dw}$ ;  $n = 4$ ). The remaining amounts, expressed relative to the initial values, are shown in Fig. 7. In all experiments, the total amounts of carbon and nitrogen per disc decreased significantly (ANOVA test,  $p < 0.01$ ) over 24 d for both *U. lactuca* discs buried in the sediment (Table 3, column 2) and the controls (data not shown). Post-hoc pair-wise tests using the Tukey HSD procedure applied to the carbon and nitrogen data after 12 d (when at least 2 replicates were available for all experiments) revealed that the degradation in the sediment resulted in a significantly greater ( $p < 0.01$ ) loss in C and N contents of *Ulva* compared to the degradation in the water (control). However, no significant differences between Experiments 1–3 in the loss of C and N were observed.

Test tubes DOC experiment: TDC and DIC concentrations in the test tubes with and without (control) *U. lactuca* were generally low (Fig. 8). Although both TDC and DIC concentrations were higher and slightly increased in tubes containing pieces of *Ulva*, the DOC concentrations were the

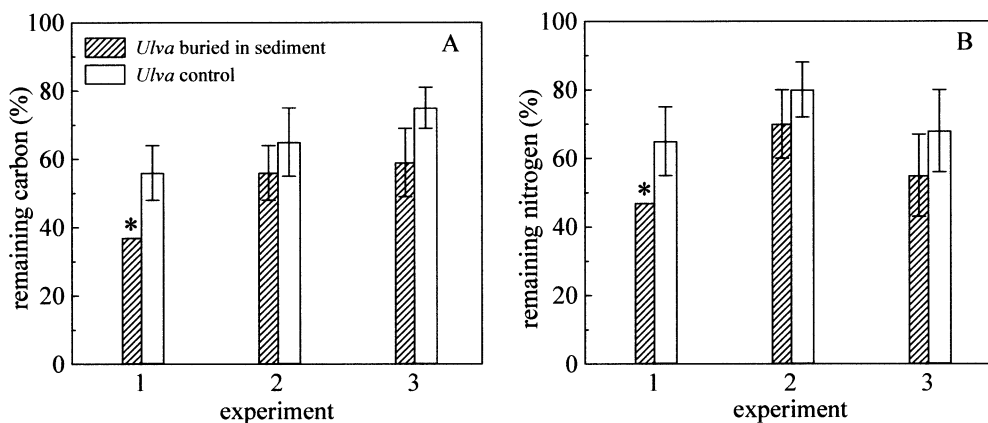


Fig. 7. (A) Remaining carbon and (B) nitrogen contents of *U. lactuca* discs after 24 d of experiments expressed as a percentage of the initial values. Error bars were calculated from  $n = 2$  samples, except for Exp. 1 (\*) where one *Ulva* disc disappeared due to ripple migration.

Table 3. Total carbon loss of *U. lactuca* derived from the carbon analysis and the OCR measurements during 24 d. Losses recorded using carbon analyses were taken as 100% values for comparison with the losses recorded using OCR measurements. Results were corrected for sediment porosity.

Exp.	Carbon analysis ( $\mu\text{g C}$ per disc)	OCR	OCR	Equivalent sediment volume ( $\text{cm}^3$ )
		measurements position of <i>U. lactuca</i> ( $\mu\text{g C}$ per $0.033 \text{ cm}^3$ )	measurements position of sediment ( $\mu\text{g C}$ per $0.033 \text{ cm}^3$ )	
1	~250 (100%)	~7.4 (3%)	~0.83	~9.6
2	~150 (100%)	~22.6 (15%)	~2.1	~2
3	~200 (100%)	~4 (2%)	~1.2	~5.4

same and remained constant during 18 d. Consequently, the increase in TDC was entirely due to the increase in DIC. Subtracting the DIC concentrations of the controls from those of the test tubes with pieces of *Ulva* and fitting the results with a linear model (dotted line in Fig. 8B), the carbon turnover of 1.13 ng C per disc of *U. lactuca* (volume of  $0.033 \text{ cm}^3$ ) in 24 d was determined.

*Consumed carbon derived from OCR measurements*—Total carbon loss derived from the OCR measurements (using Eq. 2 and data in Fig. 6A) ranged between 4.0 and 22.6  $\mu\text{g C}$ /disc. This accounts only for 15% of the carbon that was mineralized according to the carbon analysis of the discs (Table 3). The CMR values of the surrounding sediment under ripple troughs were used to estimate the POM-free sediment volume needed to account for this difference (Table 3, column 5). The corresponding sediment volumes were approx. 60–300 times larger than the assumed effective volume of the *Ulva* discs ( $0.033 \text{ cm}^3$ ).

## Discussion

In a previous study, Precht et al. (2004) showed that advection caused by the interaction of wave-driven oscillatory flow and sediment topography creates alternating patterns of oxic and anoxic regions under ripple troughs and crests, respectively. These regions vary dynamically and may thus influence the conditions (either aerobic or anaerobic) of organic matter degradation within the upper sediment layer. By determining the total oxygen uptake (TOU) of the sediment using sealable flume-channels and chamber setups, “hotspots” of organic matter degradation within the sediment and their temporal development cannot be determined because each measured signal represents a consumption rate that integrates over the entire sediment volume and a specific time period. Here, we present a technique where this lack of spatial and temporal resolutions is overcome and natural conditions can be mimicked.

*Labile POM in permeable sediments: “Hotspots” of degradation*—When oxygen-rich pore water is transported through the permeable sediment by advection, it gradually becomes depleted in oxygen with a rate determined by the

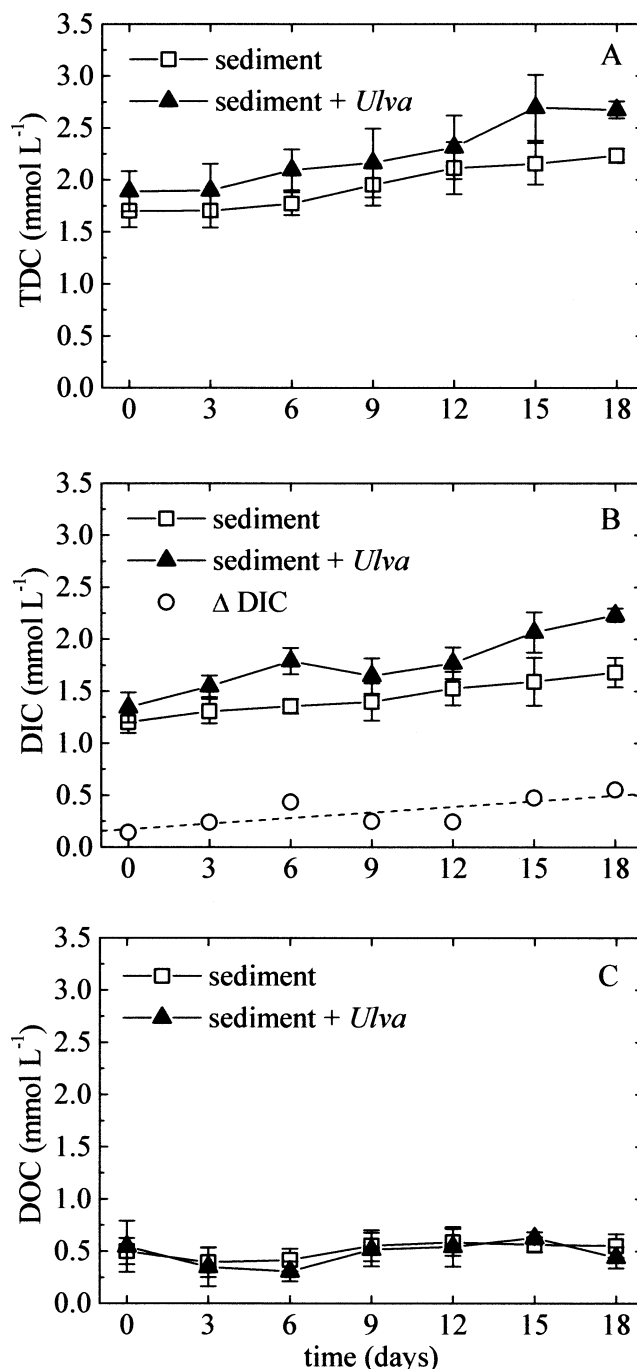


Fig. 8. (A) TDC, (B) DIC, and (C)  $\text{DOC} = \text{TDC} - \text{DIC}$  concentrations as a function of time in a test tube experiment.  $\Delta \text{DIC}$  denotes the difference between the DIC concentrations with and without *U. lactuca*. Standard deviations were calculated from  $n = 4$  samples.

pore-water flow velocity and the local volumetric OCR. No significant change in the oxygen concentration was measurable near *U. lactuca* placed directly under the ripple trough (e.g., Fig. 3A), where the pore-water velocities were high enough to deliver oxygen at rates exceeding by far the oxygen loss due to the oxygen consumption in the sediment upstream and/or at the location of the *Ulva* disc. In contrast,

sub- and anoxic zones developed when the advective oxygen delivery could not compensate the elevated OCR at or downstream the locations of *Ulva* (e.g., Figs. 3C–D), indicating a locally intense POM degradation. Similar phenomena were observed also on a larger scale, where large quantities of green algae buried in permeable sediments resulted in “black spots” at the sediment surface (Neira and Rackemann 1996).

Macrophyte decomposition typically progresses through three main stages. Initially, rapid leaching and dissolution of soluble materials associated with autolysis of cells occurs (Andersen and Hargrave 1984). The labile macromolecules of POM are subsequently transformed into dissolved organic matter (DOM) by slower, bacteria-mediated decomposition using exoenzymes (Fenchel et al. 1998). In the last phase, recalcitrant, structural carbon—e.g., cellulose or hemicellulose—are degraded at very slow rates (Castaldelli et al. 2003). This gradual decrease of the POM degradation rate was also apparent in our OCR measurements, particularly from the exponential decrease of OCR observed during the prolonged oxic conditions (Fig. 6A). The last phase with the slowest degradation rates occurred after 6–12 days. Similar decay patterns were found by Kristensen et al. (1995) and Kristensen and Holmer (2001).

The degradation rate decrease could not be confirmed directly by the carbon and nitrogen analysis, mainly due to the insufficient number of time points (limited by the number of samples). However, the carbon and nitrogen analysis did show that the degradation of *U. lactuca* in the sediment resulted in a significantly higher ( $p < 0.01$ ) carbon and nitrogen loss than in the controls degraded in water (Fig. 7). Significant differences between the three experiments could not be demonstrated, but the amounts of degraded C and N were similar for all three experiments suggesting that the aerobic and anaerobic degradation rates were comparable (Table 3). This is important because no direct rate measurements of the anaerobic processes in the used sediment are available.

*Decoupling of POM and DOM degradation in permeable sediments*—DOM is usually produced much faster by bacterial degradation of POM than it is consumed (Vetter et al. 1998). It was shown that DOM concentrations in pore water of surface sediments can be up to an order of magnitude higher than those in the overlying water (Chen et al. 1993; Martin and McCorkle 1993). In cohesive sediments the diffusive DOM flux out of the sediment was found to be up to 13% of the depth integrated sediment carbon degradation (Burdige and Homstead 1994).

In our experiments the organic carbon loss of the buried *U. lactuca* pieces derived from the OCR measurements accounted for only 4–15% of the carbon loss determined by the carbon analysis (Table 3). The discrepancy is possibly even higher considering that the effective volume of the *Ulva* disc assumed in the OCR-based calculations (a half-sphere,  $\varnothing$  0.5 cm,  $\Delta V = 0.033$  cm<sup>3</sup>) considerably overestimates the typical disc volume of 0.003 cm<sup>3</sup> ( $\varnothing$  0.5 cm, 2 cell layers  $\sim 150$   $\mu$ m thick; Bobin-Dubigeon et al. 1997). This indicates that a major fraction of the organic matter of *Ulva* was consumed not directly at the locations of the *Ulva* pieces but within the surrounding sediment after conversion into

dissolved organic matter. Such a spatial decoupling of POM and DOM degradation was enhanced by the advective pore-water flow. This is consistent with the stages of macrophyte degradation listed above that involve conversion of solid into dissolved organic matter already at the early stage of decomposition.

This spatial decoupling of POM and DOM degradation was well demonstrated in Experiment 1, where oxic degradation conditions prevailed. It is further supported by the elevated OCR values measured in the sediment downstream the positions of the *U. lactuca* discs (Fig. 5). On the other hand, no such zones were visible when diffusive conditions prevailed (e.g., in Exp. 2, OCR-data not shown).

The carbon loss calculated from the OCR measurements may not reflect accurately the degree of POM degradation under anoxic (Exp. 2) and oscillating conditions (Exp. 3). Our calculations of carbon losses using the OCR measurements are based on several simplified assumptions—especially when addressing the anoxic and oscillating conditions—which consequently result in relatively high uncertainties of the calculated numbers.

This occurs during anoxic conditions because reduced inorganic compounds (e.g., sulfide) could accumulate in the diffusive distance from the locations where the anaerobic degradation took place. As the reduced compounds can be re-oxidized, either chemically or biologically, they contribute to the sedimentary OCR. Evidence of this contribution were the persistently high and increasing OCR values at positions of POM observed after prolonged anoxic conditions (Fig. 6A, symbols connected by solid lines).

The extent to which reduced compounds are affecting the momentarily measured OCR is difficult to estimate because the contribution of re-oxidation will change during the advective phase prior the OCR measurements as well as during the OCR measurements themselves. Additionally, re-oxidation rates depend on other unknown factors such as grain size, mineralogical composition, and crystal structure of the solid phase (Bernier 1980). The anaerobic CMR values presented here were obtained under the assumption that the rate of anaerobic carbon mineralization is on average 100% of the the CMR derived from the momentarily measured OCR. Assuming a rate of 50% (e.g., Jørgensen 1982) would result in even lower OCR-derived carbon loss (e.g.,  $\sim 8\%$  of the total carbon loss determined by carbon analysis in Exp. 2). However, anaerobic degradation processes (e.g., the reduction of sulfate, Mn- and Fe oxides) and the subsequent re-oxidation of the reduced products such as H<sub>2</sub>S, Mn<sup>2+</sup>, Fe<sup>2+</sup>, and FeS by oxygen have the net stoichiometry of oxygen respiration. This means that the amount of carbon remineralized is approximated by the amount of oxygen taken up by the sediment irrespective of the mineralization pathway (Canfield et al. 1993), as formulated in Eq. 2. Therefore, the OCR values after prolonged anoxic conditions in Exp. 2 (Fig. 6A) would have to be  $\sim 7$  times higher to account for the carbon loss determined by the carbon analysis (Table 3). However, no such high OCR values were measured. A possible explanation could be that the rates were underestimated due to the experimental procedure, as advection had to be started for 4–5 h prior to each OCR measurements. During that period, the reduced solid substances (e.g., FeS precipi-

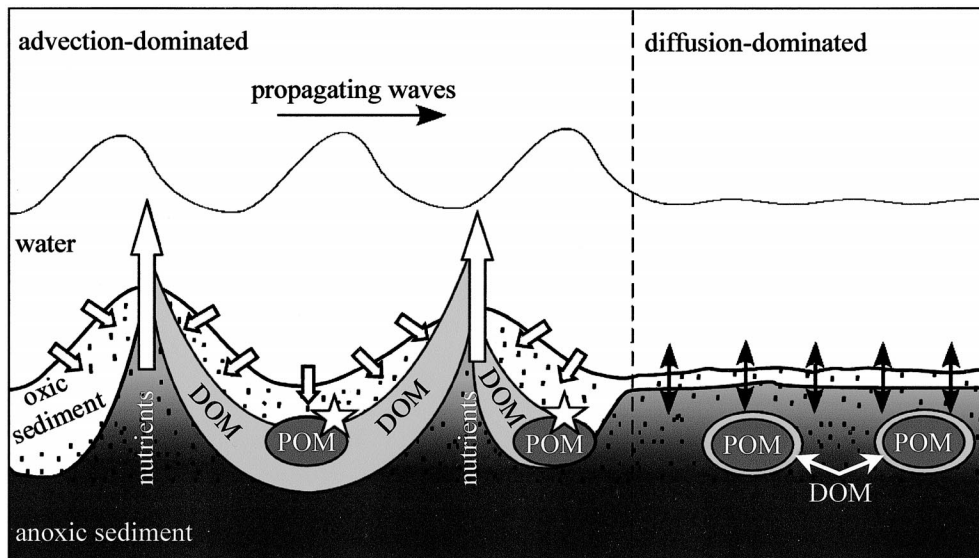


Fig. 9. Scheme of POM degradation in permeable and cohesive sediments. *Advection-dominated conditions*: Interaction of oscillatory boundary layer flow and sediment topography results in advective porewater flow. Oxygen-rich surface water is forced deep into the sediment under ripple troughs, whereas anoxic water from deeper sediment horizons leaves the sediment at ripple crests. Bacteria-mediated aerobic degradation of labile particulate organic matter (POM) is enhanced (star) in the advection affected sediment horizon (up to several cm in depth) by oxygen supply combined with transport of inhibiting products and remnants of organic matter degradation out of the sediment. Highly enhanced degradation activity can result in anoxic or suboxic (micro) sites in oxygenated sediment. The porewater flow can spatially decouple POM and the final DOM degradation, whereby bacteria in a larger sediment volume could be nourished. DOM can even be transported out of the sediment. *Diffusion-dominated conditions*: degradation of buried POM is mainly driven by anaerobic bacteria as only a thin oxic subsurface layer (typically a few mm) covers the anoxic sediment. Bacterial degradation activity can become diffusion limited. Additionally, inhibiting products can accumulate and decrease mineralization activity. DOM and nutrients can spread only in the diffusive distance, affecting a small sediment volume.

tates) could have been already oxidised and the reduced solutes could have been dispersed by the advective pore-water flow and their re-oxidation may have taken place in sediment regions invisible to the planar optode.

*Wall effect*—Because the oxygen measurements were conducted at the wave tank wall, wall effects may have affected our results. The pore-water flow during advective conditions could be slightly reduced near the wall as indicated by dye experiments in a similar set up (Huettel and Gust 1992). This would reduce the effect of advective pore-water flow on oxygen penetration and OCR near the wall, however, these effects would not affect the conclusions of our observations for advective conditions. During diffusive conditions, the diffusion field is restricted by the planar optode, which could result in possibly overestimated oxygen heterogeneities. However, comparisons of advective pore-water flow patterns at the flume wall and in the center of the flume revealed that the side wall effect had no significant influence on the advective flow pattern (Huettel et al. 1996). The oxygen distribution patterns under ripples observed in our experiments and also in experiments by Precht et al. (2004) near the flume wall agree with those distributions modeled by Shum and Sundby (1996). Furthermore, the effect of the thickness of the diffusive boundary layer on the OCR due to the presence of the wall, as described by Glud et al. (1996b), was not relevant in our case, as the derivation of OCR was based on oxygen dynamics measured inside the sediment (next to the planar optode) during purely diffusive conditions (i.e.,

no flow). Therefore, we think it is reasonable to assume that the wall effects did not have a significant influence on our results and the conclusions drawn.

*The role of advection in POM degradation*—In contrast to cohesive sediments, where diffusion is the main transport mechanism and the transport of solutes is relatively slow, DOM in permeable sediments can be transported more rapidly and spread over larger volumes of sediment when pore-water flows are present. We estimated this volume to be approx. 60–300 times the effective volume influenced by diffusion (Table 3). Consequently, the products of the degrading POM may reach and nourish more bacteria, which can result in a faster organic matter turnover. When the organic matter is located close to the sediment surface, the sedimentary produced DOM could be transported out of the sediment and remineralized in the overlying water.

This highlights a major difference between permeable and cohesive sediments as schematically depicted in Fig. 9. In permeable sediments advection not only enhances the transport and exchange of electron acceptors and substrates as well as the transport of inhibitory remnants of organic matter mineralization out of the sediment, but also decouples POM and DOM degradation and enhances the dispersion of labile DOM. In contrast, in cohesive sediments the locations of POM and the final degradation of DOM are more tightly linked because of the slow diffusive transport, with bioirrigation as an exception.

*Variable influence of buried POM on carbon cycling under natural conditions*—Under natural conditions, sediment ripples develop when the boundary flow velocity is sufficiently high. The bacteria attached to sand-grains of the top sediment layer can be exposed to rapidly changing conditions due to the tight coupling between the ripple propagation and the advective pore-water flow field (Precht et al. 2004). These bacteria have to be not only tolerant to both oxic and anoxic conditions, but also able to react instantly when their favorable conditions, possibly lasting only minutes or hours, arise. This fast reaction of the sedimentary aerobic bacterial community was detected in our experiments as up to 18 times higher OCR values at positions of *U. lactuca* compared to the surrounding sediment only minutes after the *U. lactuca* discs were placed into the sediment. That the bacteria living in the surrounding sediment and not the bacteria attached to the *U. lactuca* discs were the main degraders was confirmed by the negligible increase of DIC in a sterile sediment (dotted line in Fig. 8B).

We conclude that in the upper layers of permeable sediments, where transport is dominated by advective pore-water flow, highly elevated aerobic mineralization rates at locations of labile organic matter decomposition may lead to suboxic or anoxic (micro) sites in an otherwise oxygenated sediment. The rapid advective transport can lead to the spatial decoupling of POM degradation and the final DOM mineralisation. The temporally and spatially changing advective DOM transport can reach and nourish bacterial communities of a relatively large sediment volume, which may enhance organic matter degradation. Our experiments showed that permeable sediments have a large mineralization potential sustained by a microbial community that can react instantly to the input of labile particulate and dissolved organic material.

## References

- ALLER, R. C. 1994. Bioturbation and remineralization of sedimentary organic-matter—effects of redox oscillation. *Chemical Geology* **114**: 331–345.
- ANDERSEN, F. O., AND B. T. HARGRAVE. 1984. Effects of *Spartina* detritus enrichment on aerobic anaerobic benthic metabolism in an intertidal sediment. *Mar. Ecol. Prog. Ser.* **16**: 161–171.
- BERG, P., H. ROY, F. JANSSEN, V. MEYER, B. B. JØRGENSEN, M. HUETTEL, AND D. DE BEER. 2003. Oxygen uptake by aquatic sediments measured with a novel non-invasive eddy-correlation technique. *Mar. Ecol. Prog. Ser.* **261**: 75–83.
- BERNER, R. A. 1980. *Early diagenesis: A theoretical approach*. Princeton University Press, Princeton, New Jersey.
- BOBIN-DUBIGEON, C., M. LAHAYE, F. GUILLON, J. L. BARRY, AND D. J. GALLANT. 1997. Factors limiting the biodegradation of *Ulva* sp cell-wall polysaccharides. *Journal of the Science of Food and Agriculture* **75**: 341–351.
- BOUDREAU, B. P. 1996. The diffusive tortuosity of fine-grained unlithified sediments. *Geochim. Cosmochim. Acta* **60**: 3139–3142.
- , AND OTHERS. 2001. Permeable marine sediments: overturning an old paradigm. *EOS Trans. Am. Geophys. Union* **82**: 133–136.
- BURDIGE, D. J., AND J. HOMSTEAD. 1994. Fluxes of dissolved organic-carbon from Chesapeake Bay sediments. *Geochim. Cosmochim. Acta* **58**: 3407–3424.
- CANFIELD, D. E., AND OTHERS. 1993. Pathways of organic carbon oxidation in three continental margin sediments. *Marine Geology* **113**: 27–40.
- CASTALDELLI, G., D. T. WELSH, G. FLACHI, G. ZUCCHINI, G. COLOMBO, R. ROSSI, AND E. A. FANO. 2003. Decomposition dynamics of the bloom forming macroalga *Ulva rigida* C. Agardh determined using a C-14-carbon radio-tracer technique. *Aquatic Botany* **75**: 111–122.
- CHEN, R. F., J. L. BADA, AND Y. SUZUKI. 1993. The relationship between dissolved organic-carbon (Doc) and fluorescence in anoxic marine porewaters—implications for estimating benthic Doc fluxes. *Geochim. Cosmochim. Acta* **57**: 2149–2153.
- CRANK, J. 1975. *The mathematics of diffusion*. 2nd ed. Oxford University Press Inc.
- DE BEER, D., AND OTHERS. 2005. Transport and mineralization rates in North Sea sandy intertidal sediments Sylt-Rømø basin, Wadden Sea. *Limnol. Oceanogr.* **50**(1): 113–127.
- EMERY, K. O. 1968. Relict sediments on continental shelves of the world. *Am. Assoc. Pet. Geol. Bull.* **52**: 445–464.
- FENCHEL, T., G. M. KING, AND T. H. BLACKBURN. 1998. *Bacterial biogeochemistry. The ecophysiology of mineral cycling*, 2nd ed. Academic Press.
- FLOREK, R. J., AND G. T. ROWE. 1983. Oxygen-consumption and dissolved inorganic nutrient production in marine coastal and shelf sediments of the Middle Atlantic Bight. *Internationale Revue Der Gesamten Hydrobiologie* **68**: 73–112.
- FORSTER, S., M. HUETTEL, AND W. ZIEBIS. 1996. Impact of boundary layer flow velocity on oxygen utilisation in coastal sediments. *Mar. Ecol. Prog. Ser.* **143**: 173–185.
- GLUD, R. N., S. FORSTER, AND M. HUETTEL. 1996a. Influence of radial pressure gradients on solute exchange in stirred benthic chambers. *Mar. Ecol. Prog. Ser.* **141**: 303–311.
- , M. KUHL, O. KOHLS, AND N. B. RAMSING. 1999. Heterogeneity of oxygen production and consumption in a photosynthetic microbial mat as studied by planar optodes. *J. Phycol.* **35**: 270–279.
- , N. B. RAMSING, J. K. GUNDERSEN, AND I. KLIMANT. 1996b. Planar optodes: A new tool for fine scale measurements of two-dimensional O<sub>2</sub> distribution in benthic communities. *Mar. Ecol. Prog. Ser.* **140**: 217–226.
- HOLST, G., AND B. GRUNWALD. 2001. Luminescence lifetime imaging with transparent oxygen optodes. *Sens. Actuator B Chem.* **74**: 78–90.
- , O. KOHLS, I. KLIMANT, B. KONIG, M. KUHL, AND T. RICHTER. 1998. A modular luminescence lifetime imaging system for mapping oxygen distribution in biological samples. *Sens. Actuator B Chem.* **51**: 163–170.
- HUETTEL, M., AND G. GUST. 1992. Solute release mechanisms from confined sediment cores in stirred benthic chambers and flume flows. *Mar. Ecol. Prog. Ser.* **82**: 187–197.
- , W. ZIEBIS, S. FORSTER, AND G. LUTHER, III. 1998. Advective transport affecting metal and nutrient distribution and interfacial fluxes in permeable sediments *Geochim. Cosmochim. Acta* **62**: 613–631.
- , ———, AND ———. 1996. Flow-induced uptake of particulate matter in permeable sediments. *Limnol. and Oceanogr.* **41**: 309–322.
- JØRGENSEN, B. B. 1982. Mineralization of organic-matter in the sea bed—the role of sulfate reduction. *Nature* **296**: 643–645.
- KAUTSKY, H. 1939. Quenching of luminescence by oxygen. *Trans Faraday Soc* **35**: 216–219.
- KRISTENSEN, E., S. I. AHMED, AND A. H. DEVOL. 1995. Aerobic and anaerobic decomposition of organic matter in marine sediment: Which is fastest? *Limnol. and Oceanogr.* **40**: 1430–1437.
- , AND M. HOLMER. 2001. Decomposition of plant materials

- in marine sediment exposed to different electron acceptors ( $O_2$ ,  $NO_3^-$ , and  $SO_4^{2-}$ ), with emphasis on substrate origin, degradation kinetics, and the role of bioturbation. *Geochim. Cosmochim. Acta* **65**: 419–433.
- LI, Y. H., AND S. GREGORY. 1974. Diffusion of ions in sea-water and in deep-sea sediments. *Geochim. Cosmochim. Acta* **38**: 703–714.
- LOHSE, L., E.H.G. EPPING, W. HELDER, AND W. VAN RAAPHORST. 1996. Oxygen pore water profiles in continental shelf sediments of the North Sea: Turbulent versus molecular diffusion. *Mar. Ecol. Prog. Ser.* **145**: 63–75.
- MALAN, D. E., AND A. MCLACHLAN. 1991. In situ benthic oxygen fluxes in a nearshore coastal marine system: a new approach to quantify the effect of wave action. *Mar. Ecol. Prog. Ser.* **73**: 69–81.
- MARTIN, W. R., AND D. C. MCCORKLE. 1993. Dissolved organic-carbon concentrations in marine pore waters determined by high-temperature oxidation. *Limnol. and Oceanogr.* **38**: 1464–1479.
- NEIRA, C., AND M. RACKEMANN. 1996. Black spots produced by buried macroalgae in intertidal sandy sediments of the Wadden Sea: Effects on the meiobenthos. *J. Sea Res.* **36**: 153–170.
- POLERECKY, L., U. FRANKE, U. WERNER, B. GRUNWALD, AND D. DE BEER. 2005. High spatial resolution measurement of oxygen consumption rates in permeable sediments. *Limnol. Oceanogr.: Methods* **3**, 75–85.
- PRECHT, E., U. FRANKE, L. POLERECKY, AND M. HUETTEL. 2004. Oxygen dynamics in permeable sediments with wave-driven pore water exchange. *Limnol. and Oceanogr.* **49**: 693–705.
- , AND M. HUETTEL. 2004. Rapid wave-driven advective pore water exchange in permeable coastal sediment. *J. Sea Res.* **51**: 93–107.
- REIMERS, C. E., AND OTHERS. 2004. In situ measurements of advective solute transport in permeable shelf sands. *Cont. Shelf Res.* **24**: 183–201.
- ROWE, G. T., G. S. BOLAND, W. C. PHOEL, R. F. ANDERSON, AND P. E. BISCAEY. 1994. Deep-sea floor respiration as an indication of lateral input of biogenic detritus from continental margins. *Deep-Sea Res. Part II* **41**: 657–668.
- RUSCH, A., AND M. HUETTEL. 2000. Advective particle transport into permeable sediments—evidence from experiments in an intertidal sandflat. *Limnol. and Oceanogr.* **45**: 525–533.
- , ———, C. E. REIMERS, G. L. TAGHON, AND C. M. FULLER. 2003. Activity and distribution of bacterial populations in Middle Atlantic Bight shelf sands. *Fems Microbiology Ecology* **44**: 89–100.
- RUTGERS VAN DER LOEFF, M. M. 1981. Wave effects on sediment water exchange in a submerged sand bed. *Neth. J. Sea Res.* **15**: 100–112.
- SHUM, K. T., AND B. SUNDBY. 1996. Organic matter processing in continental shelf sediments—the subtidal pump revisited. *Mar. Chem.* **53**: 81–87.
- THAMDRUP, B., AND D. E. CANFIELD. 2000. Benthic respiration in aquatic sediments, p. 86–103. *In* O. E. R. Sala, R. B. Jackson, H. A. Mooney, and R. W. Horwarth [eds.], *Methods in ecosystem science*. Springer.
- VAN LOOSDRECHT, M. C. M., J. LYKLEMA, W. NORDE, AND A. J. B. ZEHNDER. 1990. Influence of interfaces on microbial activity. *Microbiological Reviews* **54**: 75–87.
- VETTER, Y. A., J. W. DEMING, P. A. JUMARS, AND B. B. KRIEGER-BROCKETT. 1998. A predictive model of bacterial foraging by means of freely released extracellular enzymes. *Microbial Ecology* **36**: 75–92.
- WENZHÖFER, F., AND R. N. GLUD. 2004. Small-scale spatial and temporal variability in benthic  $O_2$  dynamics of coastal sediments: Effects of fauna activity. *Limnol. Oceanogr.* **49**: 1471–1481.
- ZIEBIS, W., S. FORSTER, M. HUETTEL, AND B. B. JØRGENSEN. 1996a. Complex burrows of the mud shrimp *Callinassa truncata* and their geochemical impact in the sea bed. *Nature* **382**: 619–622.
- , M. HUETTEL, AND S. FORSTER. 1996b. Impact of biogenic sediment topography on oxygen fluxes in permeable seabeds. *Mar. Ecol. Prog. Ser.* **140**: 227–237.

Received: 2 December 2004

Accepted: 20 November 2005

Amended: 15 November 2005